Disponible en **www.hormigonyacero.com**
Hormigón y Acero 2024
https://doi.org/10.33586/hya.2023.3107

Towards the Development of a Formulation for Obtaining the Shear Strength of Concrete Composite Beams

Hacia el desarrollo de una formulación para la obtención de la resistencia a cortante de vigas compuestas de hormigón

Lisbel Rueda García[*,a], José Luis Bonet Senach[a], Pedro Fco. Miguel Sosa[a], Miguel Ángel Fernández Prada[a]

[a] *Universitat Politècnica de València, Spain*

Recibido el 30 de septiembre de 2022; revisado el 16 de enero de 2023, aceptado el 23 de enero de 2023

ABSTRACT

In the design and assessment of precast concrete beams with a slab cast on top, namely concrete composite beams, engineers still face in practice unsolved shear-related issues, such as the contribution to shear strength of the slab, the concrete strength to be considered in shear formulations or the influence of the interface between concretes in the shear behaviour. This article gives an overview of the 69 shear tests performed by the authors on monolithic and composite beams, with rectangular or T-shaped cross-section, with or without transverse reinforcement and with different concrete qualities, to experimentally analyse the issues mentioned above. The study of the shear transfer mechanisms at failure led to formulating a model for explaining the observed results. Based on this model, a shear strength predictive formulation for concrete composite beams with web reinforcement is developed in this article, which is verified with the experimental results from this research and 24 additional tests from the literature. This formulation provides more accurate predictions compared to the shear strength formulations of current codes EC2, MC-10 and ACI 318-19. The proposed model lays the foundations for the future development of a user-friendly formulation for calculating the shear strength of concrete composite beams..

KEYWORDS: reinforced concrete, composite beam, T-beam, shear strength, interface shear, predictive model.

RESUMEN

En el diseño y evaluación de vigas prefabricadas de hormigón con una losa superior hormigonada *in situ*, es decir, vigas compuestas de hormigón, los ingenieros siguen enfrentándose en la práctica a problemas no resueltos relacionados con el cortante, como la contribución de la losa a la resistencia a cortante, la resistencia del hormigón que se ha de considerar en las formulaciones de cortante o la influencia de la interfaz entre hormigones en el comportamiento a cortante. Este artículo resume los 69 ensayos a cortante realizados por los autores en vigas monolíticas y compuestas, de sección rectangular o en T, con o sin armadura transversal y con diferentes calidades de los hormigones, para analizar experimentalmente las cuestiones mencionadas anteriormente. El estudio de los mecanismos de transferencia de cortante condujo a la formulación de un modelo para explicar los resultados observados. A partir de este modelo, se desarrolla en este artículo una formulación para predecir la resistencia a cortante en vigas compuestas de hormigón con armadura de cortante, la cual se verifica con los resultados experimentales de esta investigación y 24 ensayos adicionales de la literatura. Esta formulación proporciona resultados más precisos comparados con las formulaciones de resistencia a cortante de los códigos actuales EC2, MC-10 y ACI 318-19. El modelo propuesto sienta las bases para el futuro desarrollo de una formulación fácil de usar para el cálculo de la resistencia a cortante de vigas compuestas de hormigón.

PALABRAS CLAVE: hormigón armado, viga compuesta, viga en T, resistencia a cortante, resistencia a rasante, modelo predictivo.

* Persona de contacto / *Corresponding author*:
Correo-e / *e-mail*: lisruega@gmail.com (Lisbel Rueda-García)

How to cite this article: Rueda-García, L., Bonet, J.L., Miguel, P.F., & Fernández, M.A. (2024) Towards the Development of a Formulation for Obtaining the Shear Strength of Concrete Composite Beams, *Hormigón y Acero* 75(302-303): 119-136. https://doi.org/10.33586/hya.2023.3107

Nomenclature

a	shear span
A_{sw}	area of the cross-section of the two legs of a stirrup
b_{eff}	effective shear width of the slab
b_w	web width of the concrete section
c	coefficient for the adhesive bond
c_c	effective concrete cover
$cot\theta$	cotangent of θ
$cot\theta_{int}$	cotangent of θ given by the interface shear strength
$cot\theta_{str}$	cotangent of θ given by the crushing of the compression struts
d	effective depth
d'	slab longitudinal reinforcement depth
d_b	effective depth of the precast beam
d_c	effective depth of the entire composite beam
$E_{c,b}$	modulus of elasticity of the precast beam concrete

$E_{c,s}$ modulus of elasticity of the slab concrete
E_s modulus of elasticity of reinforcement
f_c concrete compressive strength
$f_{c,b}$ concrete compressive strength of the beam measured in cylinders
$f_{c,s}$ concrete compressive strength of the slab measured in cylinders
f_{ct} concrete tensile strength
$f_{ct,b}$ concrete tensile strength of the precast beam
$f_{ct,s}$ concrete tensile strength of the slab
F_H total horizontal force transferred along the interface crack
f_y yield strength of reinforcement
f_{yw} yield strength of transverse reinforcement
h overall member height
h_s cast-in-place slab height
l_c length of the interface crack
l_{nc} length of the uncracked interface of principal span at maximum shear load
N_s axial force on slab
$Ø$ nominal diameter of a reinforcing bar
s stirrup spacing
T_l tension force of slab longitudinal reinforcement at its yield strength
T_w tension force of web reinforcement at its yield strength
V_{exp} experimental shear strength
V_{pb} precast beam shear strength
V_{pred} predicted shear strength
$V_{R,max1}$ experimental first local maximum of the shear-deflection relation
$V_{R,max2}$ experimental second local maximum of the shear-deflection relation
V_s slab shear strength
$V_{s,BF}$ slab shear strength provided by slab bending failure
$V_{s,IF}$ slab shear strength provided by interface failure
$V_{s,SF}$ slab shear strength provided by slab shear failure
α multiplier factor of interface shear strength
θ inclination of compression field struts with respect to the axis of the member
μ friction coefficient
ρ_{ic} reinforcement ratio of the reinforcing steel crossing the interface
ρ_l reinforcement ratio of tension longitudinal reinforcement
ρ_w reinforcement ratio of web reinforcement
σ_1, σ_2 principal stresses
σ_x normal longitudinal stress
τ tangential stress
τ_R interface shear strength

1. INTRODUCTION

A very common type of deck for bridges built from the mid-20th century onwards consists of precast beams with a cast-in-place slab on top, namely concrete composite beams (see Figure 1a). Given the large number of existing bridges of this type, it is especially important to study their structural behaviour. In addition, there is now a clear trend towards precast construction with reinforced concrete elements, so this type of elements is present not only in bridge structures, but also in buildings. Composite elements such as beam-and-block floors or connections of precast beams and hollow-core slabs, where the free space is filled with cast-in-place concrete, are commonly seen [1,2] (Figure 1b-c).

While the interface shear strength of concrete composite beams has been studied in many publications [3–8], their vertical shear strength has not been thoroughly analysed [9]. Full-scale concrete composite beams have been tested under shear forces and analysed in some research articles [10–13], however, some important aspects that affect the shear strength, such as the influence of the interface between concretes, the contribution of the slab to shear strength or the concrete strength to be considered in shear formulations were not analysed. Few studies have shown a close approach to those issues, the most important being those by Halicka *et al.* [1,14,15] and Kim *et al.* [9,16–18]. In particular, Halicka *et al.* developed an experimental study about the influence of interface quality on the shear strength of concrete composite beams [1,14,15], in which the possible failure mechanisms in concrete composite beams are described as well as an analytical criterion to predict the failure mechanism. Halicka points out in [14] there are few research works regarding the influence of the interface cracking on the shear strength of the composite element. Kim *et al.* [9,16–18] ran an extensive experimental programme on the shear strength of rectangular composite beams made of prestressed and non-prestressed concrete, using different strength concretes (high-strength and low-strength concrete) and adding or not steel fibres in the concrete mass. They obtained interesting results about the influence on the shear strength of these different concretes and their location at the precast beam or the slab; however, the influence of the interface was not studied since most of the specimens behaved similarly to monolithic specimens.

This lack of knowledge on the subject can be seen in the absence of a clear procedure on how to account for the slab in the shear strength of composite elements in some current codes (EC2 [19] and MC-10 [20]). ACI 318-19 [21] specifies how shear strength of composite beams can be calculated, as long as the shear at the interface is verified: using the properties of the element (precast beam or cast-in-place slab) that result in the most critical shear strength value or the properties of individual elements. Notwithstanding, relevant experimental and theoretical evidence are still needed to support the validity of these considerations for composite specimens [9,16].

With the aim of studying the different aspects related to the shear strength of concrete composite beams mentioned above, the authors developed an extensive experimental programme on concrete composite elements, which was partially published in [22–25]. The scope of this research covered specimens that showed a structural failure influenced by the existence of an interface between concretes, leaving out those with pure horizontal shear failure and monolithic behaviour, which have already been studied in multiple publications. In [22], the authors presented the results of 7 composite rectangular beams tested in shear, which were performed to characterise the interface between concretes. In [23], the authors analysed the results of 21 monolithic and composite, rectangular and T-shaped beams

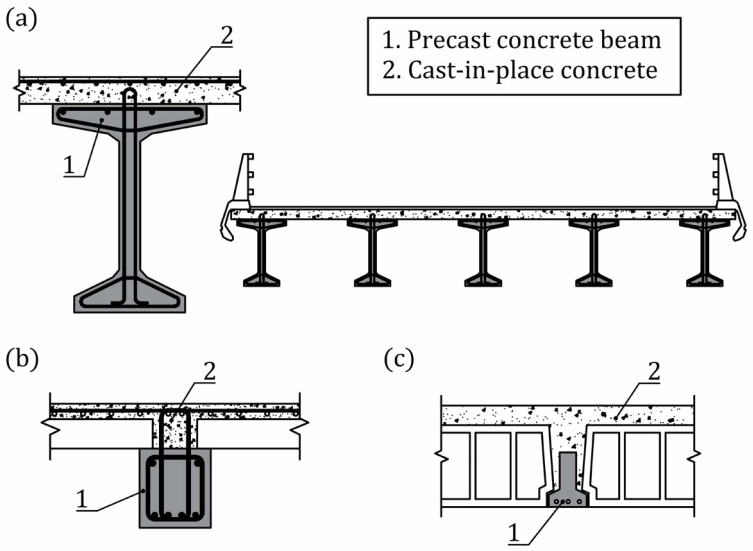

Figure 1. Examples of concrete composite structures: (a) Bridge deck made of precast beams with top cast-in-place concrete; (b) Connection of precast beam and hollow-core slab filled with cast-in-place concrete; (c) Beam-and-block floor.

without web reinforcement and analysed in depth their shear strength mechanisms. In [24], 18 monolithic and composite rectangular specimens with web reinforcement were tested in shear, and an in-depth study of the shear strength mechanisms and failure modes of the specimens was conducted. The same procedure was followed in [25], where the results of 19 monolithic and composite T-shaped specimens were analysed in shear. In the last two publications [24,25], a mechanical model was proposed based on the experimental results for explaining the shear strength of the specimens with web reinforcement.

The objective of this paper is to present in one single document the whole research carried out at the Concrete Science and Technology University Institute (ICITECH) of the Universitat Politècnica de València (UPV; Spain) for studying the shear strength of concrete composite beams. To that aim, the results of the 69 slender reinforced concrete beams tested in shear in this research, including 6 new specimens not published in [22–25] consisting of T-beams with a top cast-in-place slab, are provided. The specimens had rectangular and T-shaped cross-sections and a high longitudinal reinforcement ratio. Different parameters that influence the vertical shear strength were varied: the presence of a cast-in-place slab, the use of web reinforcement, the presence of an interface between concretes (monolithic or composite fabrication), the interface roughness and reinforcement, the flange and the slab width, the concrete compressive strength of the precast beam and the differential shrinkage between concretes. A summary of the shear strength mechanisms, the failure modes, and the effect on the shear strength of the varied parameters is presented. As a new contribution, the model for explaining the shear strength of the specimens with web reinforcement presented in [24,25] is generalised in this paper to beam geometries and reinforcement layout other than those tested by the authors. Furthermore, based on this model, a shear strength predictive formulation for specimens with web reinforcement is developed and presented herein. The experimental test results presented in this paper, together with other experimental test results from the literature, are used to verify the model. The predictions of the proposed formulation and the current code formulations are compared. This paper gives a general overview of the research, and conclusions are drawn from the analysis of the specimens as a whole.

The present research work provides relevant details about the shear transfer mechanisms of concrete composite beams subjected to shear forces, and lays the basis of a new shear strength formulation for composite specimens with web reinforcement, also applicable to monolithic T-beams, thus supporting the development in future of user-friendly shear strength formulations for this type of structures.

2. TEST PROGRAMME

2.1. Test parameters

A preliminary series (interface characterisation series) of 7 composite specimens was carried out to determine the design of the specimens so that they would fail by vertical shear and the failure would be influenced by the presence of the interface between concretes [22]. The following parameters were analysed in this first study:

- Shear reinforcement ratio (ρ_w). Three specimens were fabricated with no web reinforcement ($\rho_w = 0$) and the other four specimens with Ø8 mm two-leg stirrups spaced 250 mm (ρ_w = 0.0022), which met the maximum spacing requirements between stirrups of the design codes considered in this study [19–21] (see Table 1).
- Ratio of reinforcement crossing the interface (ρ_{ic}). As shown in Table 1, in addition to the shear stirrups, Ø8 mm two-leg interface connectors with a fork shape spaced 250 mm were placed crossing the interface in some specimens to increase their interface shear strength.
- Interface roughness. The concrete surface of the precast beam was raked before concrete hardened to get a "very rough" interface as defined in current codes [19–21] or was left as cast with no treatment after concrete vibration to get a "smooth" interface (Table 1) (see more details about the fabrication of these two surface types in Section 2.3).

TABLE 1.
Main characteristics of the specimens of the preliminary series.

Specimen	ρ_w (%)	ρic (*) (%)	Interface roughness
NOP1B2	0	0	Very rough
NOP1B2i	0	0.22	Very rough
NOP1B2ii	0	0.45	Very rough
NWP1B2	0.22	0.22	Smooth
NWP1B2i	0.22	0.22	Very rough
NWP1B2ii	0.22	0.45	Smooth
NWP1B2iii	0.22	0.45	Very rough

(*) ρ_{ic} is the ratio of reinforcement crossing the interface, which includes the stirrups in these specimens.

Note: All the specimens had cross-section type B2 (see Figure 2).

In this preliminary series the following parameters were fixed: the cross-section B2 (see Figure 2); the longitudinal reinforcement ratio (ρ_l = 4.0%); the shear span-effective depth ratio (a/d = 4.0); a design value of 30 MPa for the concrete compressive strength, both for the beam ($f_{c,b}$) and the slab ($f_{c,s}$); the time elapsed between pouring the concrete of the beam and the slab (1 day).

After this preliminary series, the following parameters that influence shear strength were experimentally studied in the main series to explain the shear strength mechanism of concrete composite elements [23–25] (note that series E1, E2 and F2 in Figure 2 were not published elsewhere):

- Shear reinforcement ratio (ρ_w). As shown in Table 2, the specimens were fabricated without web reinforcement or with Ø8 mm two-leg stirrups spaced 250 mm. No interface connectors were added.
- Presence of a slab. Some specimens (series A1 and C1 in Figure 2) were fabricated without a slab, which represented the precast beam used in composite elements, while others (series B2 and E2 in Figure 2) had a concrete slab on top of the same precast beams.
- Presence of an interface between concretes. The specimens were fabricated with one concrete (monolithic) (series A1, B1, C1, D1 and E1) or two concretes casted at different times (composite) (series B2, C2, D2, E2 and F2), as shown in Figure 2.
- Concrete compressive strength of the precast beam ($f_{c,b}$). The precast beam was fabricated with normal-strength concrete (NSC) with a design compressive strength of 30 MPa or with high-strength concrete (HSC) with a design compressive strength of 60 MPa (see Table 2).
- Flange width. The precast beam was fabricated without flanges (rectangular beams) (series A1, B1, B2, C2 and D2) or with a flange width (T-shaped beams) of 100 mm (series C1, E1, E2 and F2) or 200 mm (series D1), as observed in Figure 2.
- Slab width. The concrete slab was fabricated with the same width as the precast beam head (series B2 and E2) or with a bigger width (series C2, D2 and F2) (see Figure 2).
- Differential shrinkage between concretes. To analyse whether the different ages of the concretes had a significant influence on vertical shear strength in the specimens of this experimental programme, the concrete of the slab was poured 1 day after that of the precast beam (series NO, HO, NW and HW) or when the shrinkage of the beam concrete had stabilised (series DO and DW) (see Table 2).

The following parameters were fixed in the 62 specimens of the main test programme: ρ_l = 4.0%; a/d = 4.0; effective concrete cover-height ratio c_c/h = 0.16; the design concrete compressive strength of the slab, which was NSC of 30 MPa; a "very rough" interface in all the specimens without web reinforcement, and a "smooth" interface in the specimens with web reinforcement.

As observed, ρ_l, a/d and c_c/h were fixed for the 69 specimens of the experimental programme (preliminary series and main test programme) to make them comparable to each other. The specimens were heavily longitudinally reinforced (ρ_l = 4.0%) to avoid bending failure before shear failure in all the specimens, including those with the widest and deepest flanges, since shear strength can significantly increase due to the presence of flanges

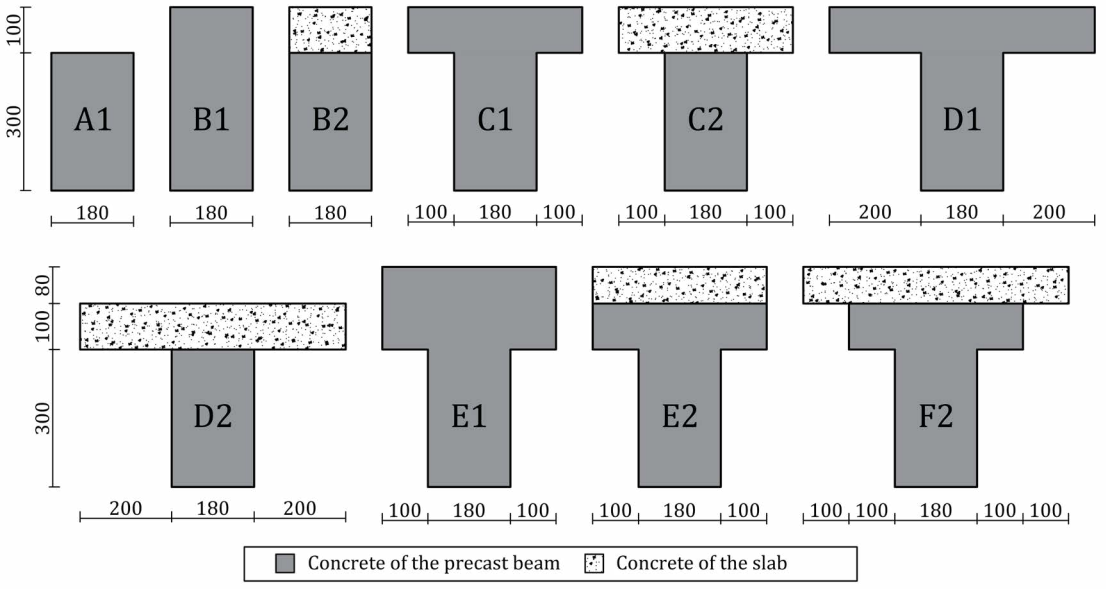

Figure 2. Cross-sectional shapes of the specimens (dimensions: mm).

TABLE 2.
Main characteristics of the specimens of the main series.

Series	ρ_w (%)	Concrete type of the beam	Concrete type type of the slab	Days between the concrete pouring of beam and slab	Number of specimens per cross-sectional									
					A1	B1	B2	C1	C2	D1	D2	E1	E2	F2
NO	0	NSC	NSC	1	2	2	2	2	2	0	2	0	0	0
HO	0	HSC	NSC	1	1	1	1	1	1	0	1	0	0	0
DO	0	NSC	NSC	134	0	0	2	0	0	0	0	0	0	0
NW	0.22	NSC	NSC	1	3	3	3	3	3	2	3	1	1	1
HW	0.22	HSC	NSC	1	2	2	2	2	2	2	2	1	1	1
DW	0.22	NSC	NSC	134	0	0	2	0	0	0	0	0	0	0

[2]. They were slender, with a/d of 4.0, to foster shear failure mainly governed by beam shear-transfer actions [26,27], thus avoiding the shear resisted by the arching action. All the specimens had the same effective concrete cover-height ratio c_c/h = 0.16 to avoid its influence on shear strength.

2.2. Test specimens

Four-point bending tests were performed in the specimens. Two point loads 0.40 m apart divided the length between supports in two spans: the principal span, where shear failure

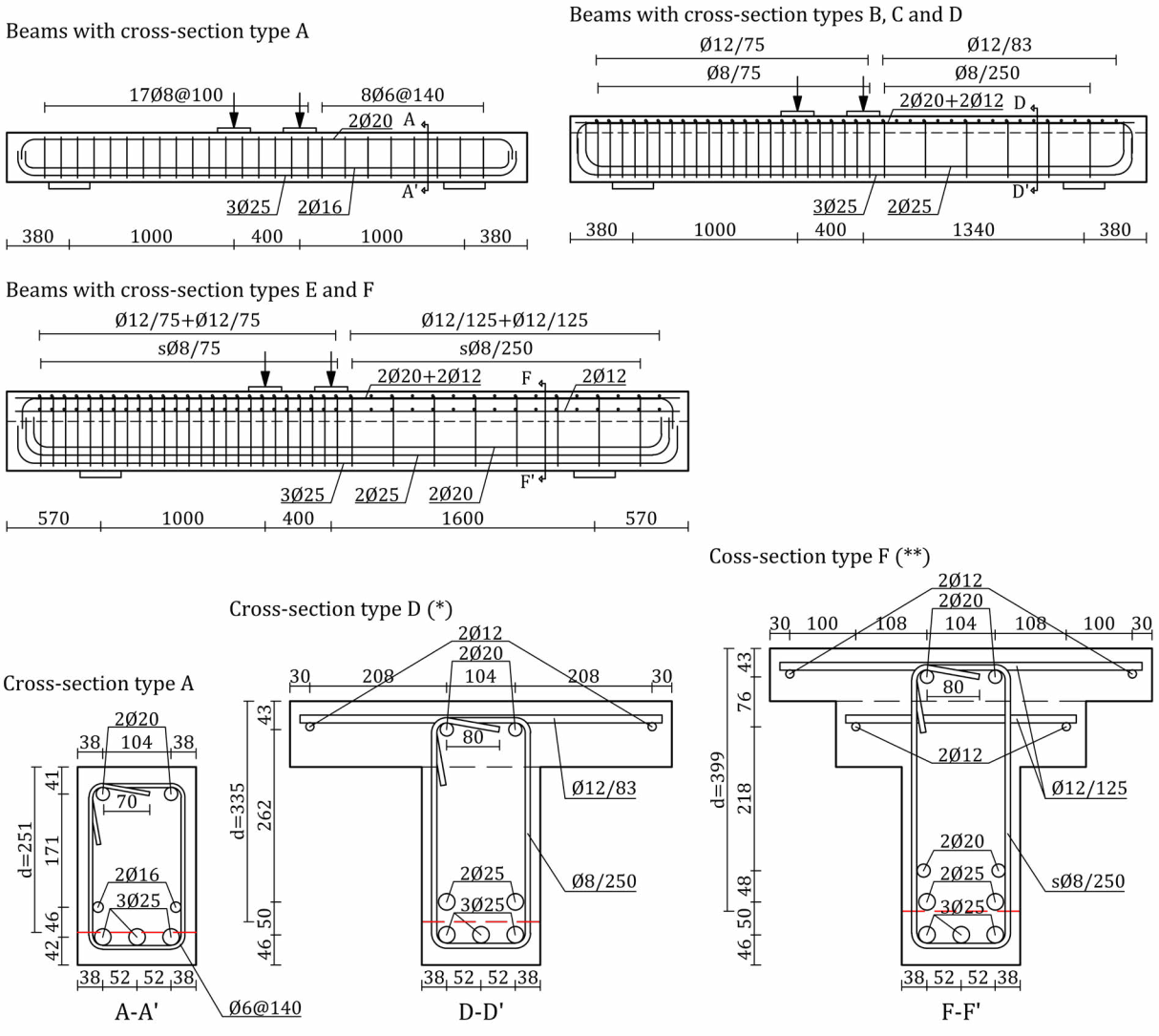

(*) Beams with cross-section types B and C have the same reinforcement; only the flange transverse reinforcement differs, which is not present in B and is adapted to the flange dimensions in C.
(**) Beams with cross-section type E have the same reinforcement; only the flange transverse reinforcement differs, which is adapted to the flange dimensions.

Figure 3. Dimensions and reinforcement of the test specimens (dimensions: mm).

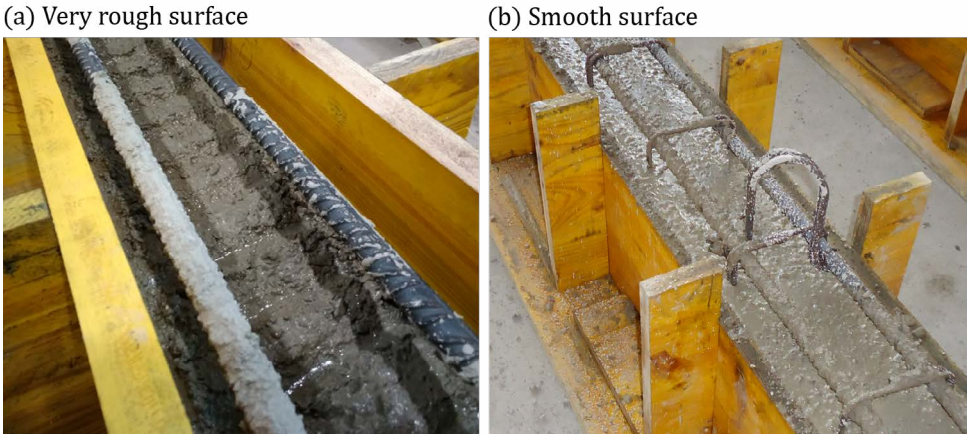

Figure 4. Pictures of the concrete surface before pouring the concrete of the slab: (a) "Very rough" surface; (b) "Smooth" surface.

was expected, whose length was 1.00 m for series A, 1.34 m for series B, C and D or 1.60 m in series E and F (see Figure 3); the over-reinforced span, which was 1.00-metre long in all the specimens and had additional shear reinforcement to prevent its shear failure. The cross-sectional dimensions of the specimens are shown in Figure 2.

Figure 3 shows the reinforcement layout of series A, D (same as series B and C) and F (same as series E) with web reinforcement (series NW, HW and DW). The specimens without web reinforcement (series NO, HO and DO) had identical reinforcement as those with web reinforcement but without the stirrups of the principal span.

Table 1 and Table 2 show the main characteristics of the preliminary and the main series, respectively. The nomenclature used to identify the specimens was *xyPzkj(l)(m)*, where:

- "*x*" is: N in the specimens fabricated with NSC at the precast beam and the slab; H in the specimens with HSC at the precast beam; D in the specimens in which more than 1 day elapsed between the concrete casting of the beam and the slab.
- "*y*" refers to the presence of web reinforcement: O for the specimens without web reinforcement; W for the specimens with web reinforcement.
- "*Pz*" refers to the concrete pouring batch, since the fabrication process was conducted in batches of up to 7 beams: P1 to P5 for specimens without web reinforcement; P1 to P8 for specimens with web reinforcement.
- "*k*" refers to the cross-section type (A to F in Figure 2).
- "*j*" refers to the number of concretes used: 1 for monolithic beams, 2 for composite beams.
- "*l*" ("a" or "b") is used only when more than one specimen with the same previously described characteristics was fabricated.
- "*m*" ("i", "ii" or "iii") is used only to identify the specimens of the preliminary test programme.

2.3. *Fabrication and materials*

The specimens were fabricated in batches of up to 7 beams. First, concrete of the precast beam was poured (see Figure 2). In

TABLE 3.
Average values of the concrete properties of the beam and the slab at the age of tests.

Series	Fabrication batch	$f_{c,b}$ (MPa)	$f_{c,s}$ (MPa)	$E_{c,b}$ (GPa)	$E_{c,s}$ (GPa)	$f_{ct,b}$ (MPa)	$f_{ct,s}$ (MPa)
NO	P1	32	31	35	32	2.41	2.72
	P2	40	34	33	26	2.24	2.77
	P3	31	38	28	31	2.48	2.40
HO	P4	62	31	37	30	3.51	2.36
DO	P5	29	37	25	31	2.44	2.82
NW	P1	33	32	34	38	2.61	2.27
	P2	38	34	33	31	2.91	2.75
	P3	32	37	33	34	2.58	3.21
	P4	39	33	28	28	2.90	2.59
	P7	24	-	23	-	1.90	-
	P8	25	26	22	24	1.93	2.18
HW	P5	43	21	25	20	2.50	2.01
	P6	52	36	28	29	2.86	3.01
	P9	67	30	33	26	4.06	2.69
DW	P7	29	37	25	31	2.44	2.82

Note: Table 5 shows the specimens that were made in each fabrication batch.

the composite specimens with "very rough" interface, the surface was raked before concrete hardened, so dents of approximately 6 mm deep between peak to valley and a maximum spacing between valleys of 40 mm were made (according to the "very rough" definition of current codes [19–21]) (see Figure 4a). In the specimens with "smooth" interface, no further treatment was carried out in the principal span after vibration (Figure 4b). The over-reinforced span of all the composite specimens was raked to improve its interface shear strength. Secondly, concrete of the slab was poured in the composite specimens 1 day after the precast beam concrete was cast, except for the DO and DW series specimens, where the concrete of the slab was poured when the instrumentation revealed that the shrinkage of the precast beam concrete had stabilised (see Table 2).

The main properties of the concretes used in the specimens of each fabrication batch are summarised in Table 3. The table shows for each batch the average values of the concrete compressive strength of the beam and slab ($f_{c,b}$ and $f_{c,s}$, respectively), the modulus of elasticity of concrete of the beam and slab ($E_{c,b}$ and $E_{c,s}$, respectively) and the tensile strength of the concrete of the beam and slab ($f_{ct,b}$ and $f_{ct,s}$, respectively), measured according to UNE-EN 12390 [28–30] at the testing age, which was approximately 28 days after the concrete of the slab was poured. Two concrete cylinders of each concrete (beam and slab) were tested every consecutive day a specimen was tested for obtaining each mechanical property. Consequently, the results shown in Table 3 are the average of testing a minimum of four and a maximum of six concrete cylinders for each property. NSCs had 325 kg/m³ of Portland cement, a water-cement ratio of 0.52 and a maximum aggregate size of 10 mm. HSCs had 500 kg/m³, 0.44 and 10 mm, respectively.

The yield strength (f_y) and the modulus of elasticity (E_s) of the reinforcing steel measured according to UNE-EN ISO 6892 [31] are shown in Table 4. It should be noted that, except for the preliminary series (NOP1 and NWP1), the steel of the stirrups (8-millimetre diameter bars) was the same, to avoid the influence of a variation in yield strength when comparing test results.

2.4. Test setup and instrumentation

Figure 5 shows the test setup. The load was applied by a 1200 kN hydraulic actuator through a steel frame which divided it into two point loads. The frame was connected to a hinge joint to keep the load vertical, and two loading steel plates (200x200x30 mm) were arranged to spread the load over the concrete. The specimens laid on steel plates (250 mm width) equipped with a steel balls bed to minimise the horizontal reaction. The load was displacement controlled at a speed of 0.20 mm/s.

Figure 5. Example of the experimental setup.

The applied load and the reactions were measured with three 1000 kN load cells. The vertical displacement at the support sections and below the point load closest to the principal span were measured with displacement transducers (LVDTs). Four LVDTs were placed horizontally at the interface between concretes to measure the slip at the interface. 120 Ω resistance and 2 mm length strain gauges were glued on some reinforcing bars: on the bottom longitudinal reinforcement at different cross-sections, including that below the point load; on the top longitudinal reinforcement at the cross-section below the point load; at the mid-length of the two legs of the principal span stirrups. Two (in rectangular specimens) or three (in T-shaped specimens) 120 Ω resistance and 60 mm length strain gauges were located on the top concrete surface at two different cross-sections of the principal span. The concrete surface was prepared to use DIC (Digital Image Correlation) with the images of two digital cameras that took pictures at a rate of 0.5 Hz. Further details about the instrumentation elements and their location can be found in [22–25].

TABLE 4.
Average values of the transverse and longitudinal reinforcement properties, for each reinforcing bar diameter (diameter in mm).

Series	f_y (MPa)						E_s (GPa)					
	6	8	12	16	20	25	6	8	12	16	20	25
NOP1, NWP1	534	534	-	-	534	556	227	189	-	-	206	197
NOP2, NOP3, HOP4, DOP5, NWP2, NWP3, NWP4, DWP7	-	538	533	561	585	557	-	203	207	240	192	199
NWP7, NWP8, HWP5, HWP9	-	538	529	545	541	548	-	203	196	230	194	235
HWP6	-	538	527	531	560	574	-	203	201	231	190	237

3. TEST RESULTS AND DISCUSSION ON THE EFFECT OF TEST PARAMETERS ON SHEAR STRENGTH

3.1. Preliminary series

The aim of this preliminary series, presented in [22], was to define the required interface roughness and the ratio of reinforcement crossing the interface that led to a shear failure of the specimens influenced by the presence of the interface, i.e., where the diagonal shear cracks deflected horizontally upon reaching the interface and penetrated the slab afterwards, thus avoiding pure horizontal shear failure or monolithic shear-resistant behaviour (i.e., cracks cross the interface without developing horizontally along it, as Halicka observed in [14]).

During the design of these specimens, their predicted failure mode was determined by comparing the horizontal shear strength with the vertical shear strength given by the current design code formulations [19–21]. Thus, 7 different designs were selected (see Table 1). Of the three specimens without shear reinforcement, NOP1B2 and NOP1B2i were expected to reach their horizontal shear failure before their vertical shear failure. Among the four specimens with shear reinforcement, the horizontal shear failure was expected only in the specimens with smooth interface (NWP1B2 and NWP1B2ii). However, all the specimens had a vertical shear failure (their experimental shear strengths (V_{exp}) are shown in Table 5) [22]. Pure horizontal shear failure or delamination [14], where the diagonal shear crack deviates along the interface and does not penetrate the top slab, did not occur in any specimen. Among the specimens without shear reinforcement, specimen NOP1B2, was the only one showing diagonal cracking influenced by the presence of the interface between concretes (see Figure 6). On the contrary, the other two specimens showed a crack pattern similar to that of monolithic specimens, in which the interface plane did not deviate the diagonal shear crack. In the specimens with shear reinforcement, only the crack patterns of those specimens with a smooth interface were influenced by the presence of the interface. It was also observed in the specimens with additional interface reinforcement (NOP1B2i, NOP1B2ii, NWP1B2ii and NWP1B2iii) that the fork connectors placed to increase their horizontal shear strength had an additional unintended effect which was increasing their vertical shear strength, since they interacted with the diagonal compression field in the web. In the specimens without shear reinforcement, the shear strength increased by 77% when the ratio of reinforcement crossing the interface (ρ_{ic}) was 0.0022 (see Table 1) and by 92% when ρ_{ic} = 0.0045. In the specimens with shear reinforcement (ρ_w = 0.0022), the additional interface reinforcement (ρ_{ic} = 0.0045) increased shear strength by 24% when the interface was "smooth" and by 73% when the interface was "very rough".

Therefore, the remaining tests of the experimental programme were designed without interface connectors additional to the shear reinforcement, since horizontal shear failure did not take place in any specimen, with a "very rough" interface for the specimens without web reinforcement and with "smooth" interface for specimens with web reinforcement.

TABLE 5.
Shear strength of the 69 test specimens.

Series	FB	Specimen	V_{exp} (kN)	Failure mode	Series	FB	Specimen	V_{exp} (kN)	Failure mode	Series	FB	Specimen	V_{exp} (kN)	Failure mode
NO	P1	NOP1B2	91	CSC	NW	P1	NWP1B2	206	SF	NW	P7	NWP7D1b	197	SF
		NOP1B2i	161	CSC			NWP1B2i	181	DT		P8	NWP8E1	259	SF
		NOP1B2ii	175	CSC			NWP1B2ii	255	SF			NWP8E2	241	IF
	P2	NOP2A1	75	CSC			NWP1B2iii	313	SC			NWP8F2	223	IF
		NOP2B1	88	CSC		P2	NWP2A1	158	SC	HW	P5	HWP5A1	144	SC
		NOP2C1	72	CSC			NWP2B1	181	SC			HWP5B1	207	SC
		NOP2C2	94	CSC			NWP2B2	186	SF			HWP5B2	172	SC
		NOP2D2	84	CSC			NWP2C1	221	SF			HWP5C1	238	SF
	P3	NOP3A1	62	CSC			NWP2C2	177	BF			HWP5C2	166	SF
		NOP3B1	81	CSC			NWP2D2	216	IF			HWP5D1	200	SF
		NOP3B2a	70	CSC		P3	NWP3A1	128	SC			HWP5D2	173	BF
		NOP3B2b	86	CSC			NWP3B1	174	SC		P6	HWP6A1	(*)	SC
		NOP3C1	79	CSC			NWP3B2	169	BF			HWP6B1	199	DT
		NOP3C2	86	CSC			NWP3C1	187	SF			HWP6B2	186	SF
		NOP3D2	85	CSC			NWP3C2	172	BF			HWP6C1	231	SF
HO	P4	HOP4A1	86	CSC			NWP3D2	176	BF			HWP6C2	222	SF
		HOP4B1	93	CSC		P4	NWP4A1	153	SC			HWP6D1	246	SF
		HOP4B2	101	CSC			NWP4B1	168	DT			HWP6D2	209	IF
		HOP4C1	90	CSC			NWP4B2	191	DT		P9	HWP9E1	327	SF
		HOP4C2	86	CSC			NWP4C1	200	SF			HWP9E2	315	IF
		HOP4D2	99	CSC			NWP4C2	197	SF			HWP9F2	315	IF
DO	P5	DOP5B2a	88	CSC			NWP4D2	229	IF	DW	P7	DWP7B2a	167	BF
		DOP5B2b	89	CSC		P7	NWP7D1a	195	SF			DWP7B2b	179	SF

(*)Vexp could not be measured due to an error detected during the test process.
FB = fabrication batch; CSC = critical shear crack formation; DT = diagonal tension failure; SC = shear-compression failure; BF = slab bending failure; SF = slab shear failure; IF = interface failure.

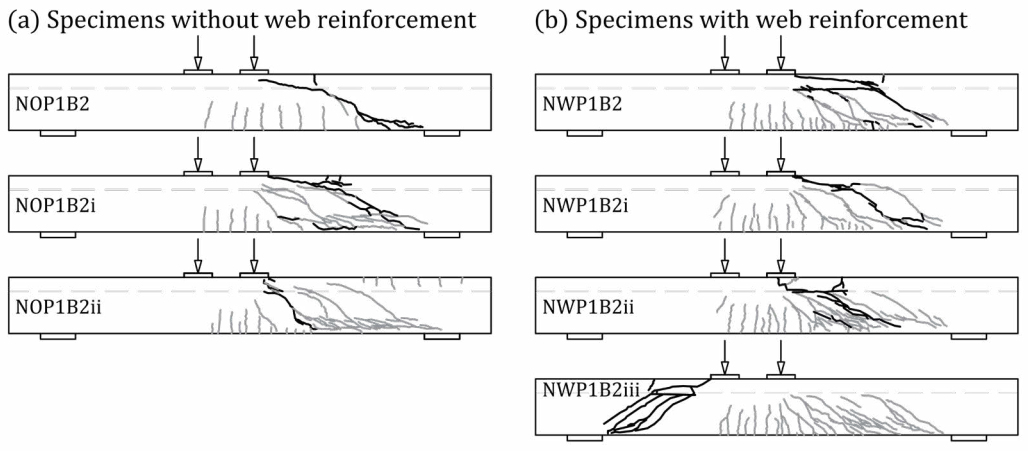

Figure 6. Crack patterns of the preliminary test programme specimens.

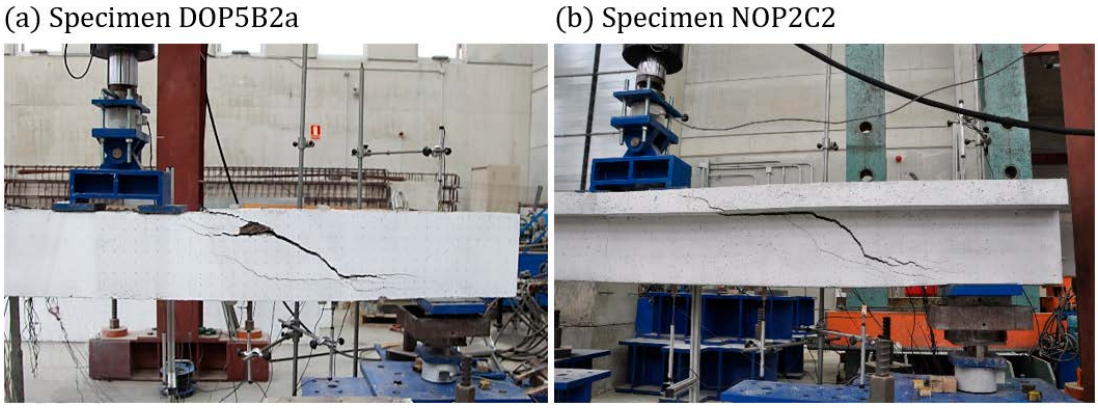

Figure 7. Examples of shear tests on specimens without web reinforcement: (a) Composite rectangular specimen DOP5B2a; (b) Composite T-shaped specimen NOP2C2.

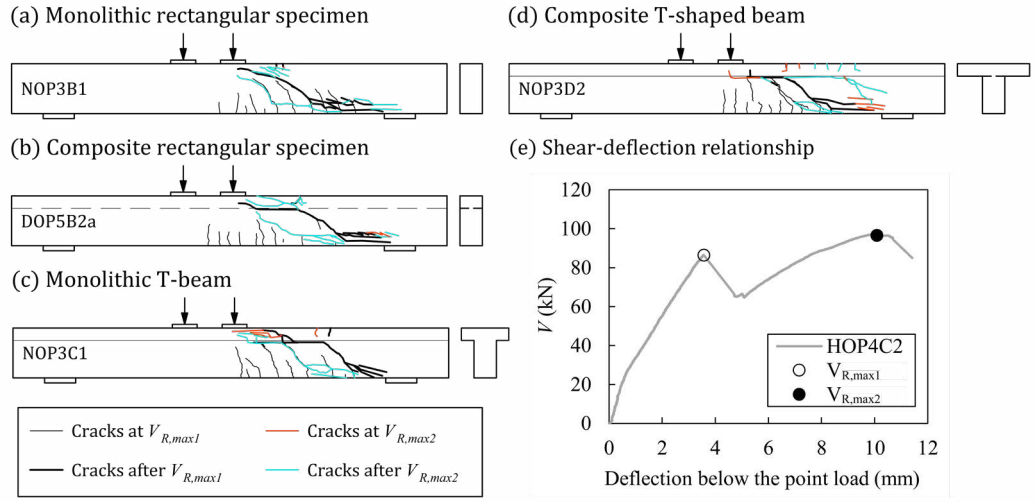

Figure 8. Examples of crack patterns of beams without web reinforcement and example of shear-deflection curve: (a) monolithic rectangular specimen; (b) composite rectangular specimen; (c) monolithic T-beam; (d) composite T-shaped beam; (e) shear-deflection relationship for the specimen HOP4C2 differentiating between VR,max1 and VR,max2 (adapted from [23]).

Regarding the horizontal shear strength provided by code formulations, the conclusion drawn from these tests was that the codes greatly underestimate the horizontal shear strength of concrete interfaces (further information about the predicted horizontal shear strength can be found in [22]).

3.2. *Main series*

The main grouping of the test specimens for analysing the results were specimens with and without web reinforcement, since they showed different shear strength mechanisms.

3.2.1. Specimens without web reinforcement

21 monolithic and composite specimens of series NO, HO and DO, with different cross-sectional shapes were analysed in [23], including the specimen NOP1B2 from the preliminary test programme, since it had the same roughness and reinforcement characteristics. Their experimental shear strengths are shown in Table 5. The most relevant parts of this analysis are presented in the following.

Regarding the crack patterns at failure, all the specimens showed a bending crack that developed diagonally towards the point load, which turned out to be the critical shear crack (CSC failure mode in Table 5). See two examples in Figure 7. The interface between concretes in the composite rectangular and T-shaped specimens (B2, C2 and D2) and the width change plane in the monolithic T-shaped specimens (C1), deviated the CSC horizontally along it before progressing across the top of the beam, as shown in the examples of Figure 8.

The formation of the CSC caused a load drop. However, it did not cause the collapse of most of the specimens, and a second local maximum in shear was reached afterwards (see $V_{R,max2}$ in Figure 8e). The second maximum shear value was sometimes higher than the first ($V_{R,max1}$ in Figure 8e) and may be explained by an arching action mechanism developed above the CSC, which was described in [27]. The crack patterns revealed that the specimens in which the CSC left a wide enough depth of the compression chord intact reached higher second local maximums in shear. However, no relationship was found between the initial characteristics of the specimens and the depth of the compression chord that remained intact after the CSC formation. The high ρ_l in tension in the beams of this experimental programme (4.0%) could be one of the reasons why the high arch effect could develop in some of the specimens. On the other hand, the membrane effect due to the large deflection of the longitudinal tie could also contribute to the shear resistance. In the specimens of this experimental programme, it was considered unsafe to take the absolute maximum shear value as the shear strength, since the shear transfer mechanisms for explaining that behaviour were not clear. Thus, the first local maximum in shear was taken as the shear strength of the element, which is the value shown in Table 5.

The test parameters defined in Section 2.1 were analysed by comparing the shear strengths of different specimens where only one parameter is varied. The observations of this analysis were as follows (further details can be found in [23]):

- Presence of a slab. If the average shear stresses are compared, the specimens of series B1 resisted 7% less (on average for all the fabrication batches of series NO) than the specimens of series A1, which was due to the size effect. The specimens of series B2 resisted 5% less than the specimens of series A1. Given both values are similar, this decrease in the average shear stress of B2 beams was also attributed to the size effect and not to the presence of an interface between concretes. Consequently, placing a slab of depth h_s increased shear strength by approx. the same as an increase of h_s in the effective depth of the beam. Since the interface conditions are key for the contribution of the slab to the shear strength, the observed behaviour is possible provided that the horizontal shear resistance at the interface is verified.
- Presence of an interface between concretes. The interface between concretes modified the crack pattern with respect to that of monolithic specimens by deviating the direction of the CSC. Regarding the shear strength, little differences were found in Vexp between the monolithic and the composite specimens with the same cross-sectional shape.
- Concrete compressive strength of the precast beam. The specimens where the beam was made of HSC showed slightly greater shear strength than those made of NSC (4% on average). By comparing the specimens made of HSC and NSC, it was observed that the formation of the critical shear crack was mostly governed by the strength of the web concrete, while the contribution of the arching action mechanism to the shear strength depended on the strength of the slab concrete.
- Flange and slab width. The rectangular and T-shaped specimens had similar first local maximums in shear, because shear strength was mainly governed by the shear transfer actions that occurred at the web of the beam. Afterwards, the specimens type D, with wider flanges, reached higher second local maximums in shear than the specimens type C.
- Differential shrinkage between concretes. Differential shrinkage in series DO did not have a significant influence on the vertical shear capacity of the composite beams without shear reinforcement of this test programme.

3.2.2. Specimens with web reinforcement

The 42 specimens with web reinforcement and the specimen NWP1B2 from the preliminary series [22] were analysed

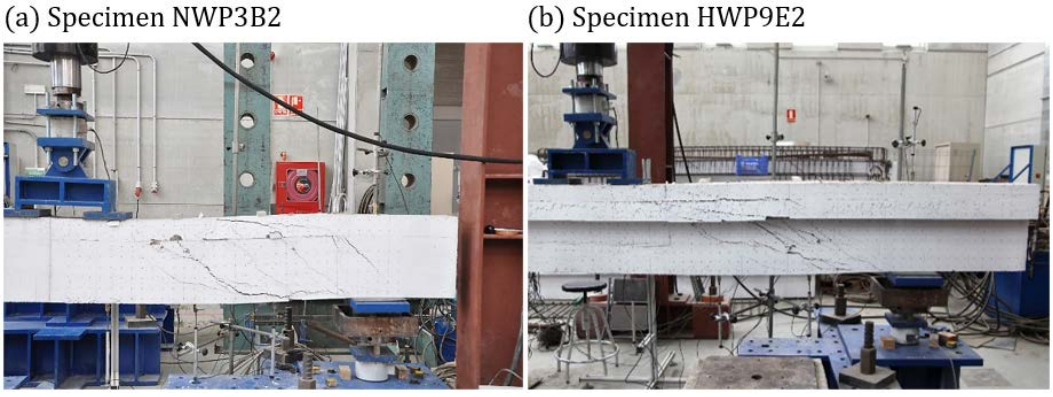

Figure 9. Examples of shear tests on specimens with web reinforcement: (a) Composite rectangular specimen NWP3B2; (b) Composite T-shaped specimen HWP9E2.

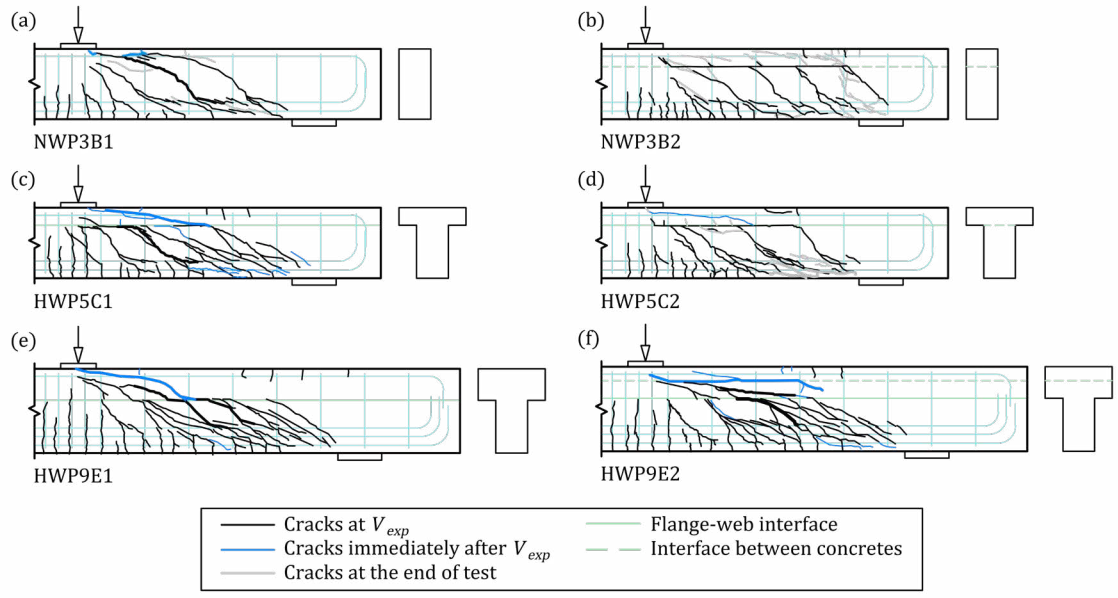

Figure 10. Crack pattern examples of specimens with web reinforcement: (a) monolithic rectangular specimen B1 [24]; (b) composite rectangular specimen B2 [24]; (c) monolithic T-shaped specimen C1 [25]; (d) composite T-shaped specimen C2 [25]; (e) monolithic T-shaped specimen E1; (f) composite T-shaped specimen E2.

(see further results from series A1, B1 and B2 in [24] and from series C1, C2, D1 and D2 in [25]). In this section, the most important parts of the analysis of the specimens with web reinforcement are summarised.

Unlike the specimens without web reinforcement, these specimens showed one maximum shear value.

Regarding the crack patterns, big differences were found between monolithic rectangular specimens and specimens with an interface between concretes (composite specimens) or a cross-section width change (T-beams). In most specimens, the interface or the cross-section width change plane modified the crack pattern of the specimens versus that of monolithic rectangular beams by forcing diagonal cracks to develop along that weak plane (see the pictures of Figure 9). Representative examples of these crack patterns are shown in the drawings of Figure 10.

The differences in the crack patterns had a big influence on the shear strength mechanisms developed by the specimens and, consequently, on their shear strengths, whose values are shown in Table 5.

The shear strength mechanisms of the specimens with one weak plane (interface between concretes or cross-section width change) were analysed. The crack at the weak plane divided the transmission of the shear force to the supports into two load paths. In the monolithic T-beams (series C1, D1 and E1) one shear path was the beam web and the other shear path were the flanges. In the composite specimens (series B2, C2 and D2), the lower path was the precast beam, and the upper path was the slab. Shear forces at the lower path were seen to be mainly resisted by the web reinforcement, while the upper path behaved as a member without shear reinforcement. Both shear transfer mechanisms were connected through the crack at the weak plane, by means of the aggregate interlock along the crack and the dowel action of the web reinforcement. The failure of the specimens was given when the upper mechanism or the interface failed. Three failure modes were observed: slab bending failure (BF), slab shear failure (SF) or interface failure (IF).

- BF was observed when specimens showed a long crack along the weak plane that covered almost all the shear span (e.g., specimen of Figure 10b). Flexural cracks appeared at the top of the slab close to the support section and a gradual drop of the shear-deflection curve was observed, characteristic of a ductile bending failure (see Figure 11a).
- SF was observed in specimens with a smaller crack extension along the weak plane when a sudden diagonal crack crossed the slab in direction to the point load (e.g., specimens of Figure 10c-e) and a marked load drop was recorded, characteristic of a brittle shear failure (see Figure 11b).
- IF was observed in those specimens that showed a short interface crack before reaching their shear strengths. After this peak load, the crack extended along the interface towards the support, leading to a marked load drop, and no new strength mechanism developed to increase this load (see Figure 11c).

These failure modes, identified in the specimens with web reinforcement, are shown in Table 5. Additionally, Table 5 indicates the failure mode of the monolithic rectangular specimens as well as the composite rectangular specimens that failed in shear in the same way as a monolithic beam (i.e., where the presence of the interface did not modify the cracking pattern nor the shear strength mechanisms). In all these specimens, the compression chord failed once the web reinforcement had yielded. Consequently, the two observed failure modes in these specimens were those commonly known (e.g., see [16]) as diagonal tension failure (DT in Table 5) (see for example the specimen NWP1B2i in Figure 6) and shear-compression failure (SC in Table 5) (e.g., specimen NWP3B1 in Figure 10a).

The specimens E2 and F2 with two weak planes (the interface between concretes and the cross-section width change) showed a small extension of the cracks at the cross-section width change of the T-beam (see Figure 10f) until the maximum load, which divided the shear transmission into two load

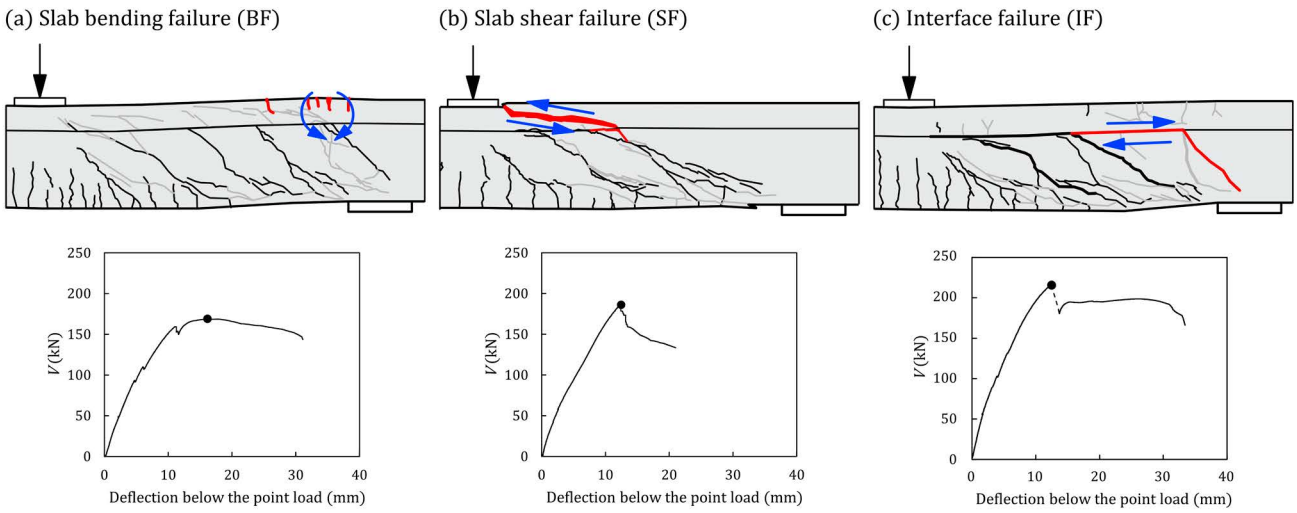

Figure 11. Representative examples of the three failure modes and their shear-deflection curves: (a) Slab bending failure (BF) (specimen NWP3B2); (b) Slab shear failure (SF) (specimen HWP6B2); (c) Interface failure (IF) (specimen NWP2B2).

paths. The lower path was the web of the T-beam, and the upper path were the flanges of the T-beam and the slab. After the peak load, the upper path failed due to the formation of a horizontal crack towards the support at the interface between the T-beam and the slab, due to the interface reaching its interface shear strength before the specimen reached its strength by SF. Therefore, the specimens failed by IF.

Further information about this analysis of the shear strength mechanisms can be found in [24,25].

Regarding the effect of the varied parameters on the shear behaviour of these specimens, the following observations were made:

- Shear reinforcement ratio. As expected, the specimens with web reinforcement reached higher V_{exp} than the specimens without web reinforcement. The increase may be explained by the activation of different shear transfer actions after the formation of the CSC. The strain gauges located on the stirrups of the shear span showed they reached their yield strength, which proved the contribution of the stirrups. The increase of V_{exp} due to the presence of web reinforcement was 117% on average for each cross-sectional shape.
- Presence of a slab. The average shear stresses of series B1 and B2 were, respectively, 10% and 6% lower (on average for all the fabrication batches of series NW) than that of specimens of series A1. Since both values are similar, this decrease in the average shear stress of B2 specimens was attributed to the size effect and not to the presence of an interface. If the average shear stresses of specimens E1 and E2 of series NW are compared to those of series C1, the shear strengths decreased by 8% and 15%, respectively (a shear-effective area of the slab that increases 45° from the cross-section width change, as in [25], is considered). Since these values are quite different, in specimens E2, with two weak planes, not only the size effect decreased shear strength but also the presence of an interface between concretes.
- Presence of an interface between concretes. As indicated above, the interface modified the crack pattern, however, in composite rectangular specimens with similar concrete compressive strength in both the beam and slab, the interface did not significantly modify their shear strength, regardless of the interface presenting more or less cracking. In the T-shaped specimens, the presence of an interface between concretes decreased the shear strength of the specimens, since the greater interface cracking resulted in less resistant failure mechanisms, such as slab bending failure in the specimens that showed extended interface cracking.
- Concrete compressive strength of the precast beam. The monolithic specimens made with HSC concrete had 11% higher shear strength than the monolithic specimens made with NSC (on average for each cross-sectional shape). The composite beams with higher concrete compressive strength in the precast beam than in the slab showed lower shear strengths than their homologous monolithic specimens made of the same concrete as that of the precast beam (12% lower strength on average). Another important observation derived from varying the concrete compressive strength of the beam was that the shear strength of the tested specimens that presented an extended interface cracking did not depend on the concrete compressive strength of either the beam or the slab, since their shear strength was given by the bending failure of the slab. On the contrary, the shear strength of the specimens in which interface cracking was short depended on the concrete compressive strength of the slab, since the shear strength was given by the slab failing in shear.
- Differential shrinkage between concretes. It was again verified that a marked differential shrinkage between concretes did not significantly modify the shear strength of the composite beams in this experimental programme in relation to that of those specimens with reduced differential shrinkage.
- Flange and slab width. On one hand, in the specimens with slab shear failure (all the monolithic specimens and some composite specimens), the presence of flanges increased shear strength. In this research work specimens, the shear strength increased approx. 17% due to the presence of flanges, which is the same increase in the shear-effective area as when considering an effective slab width that equals

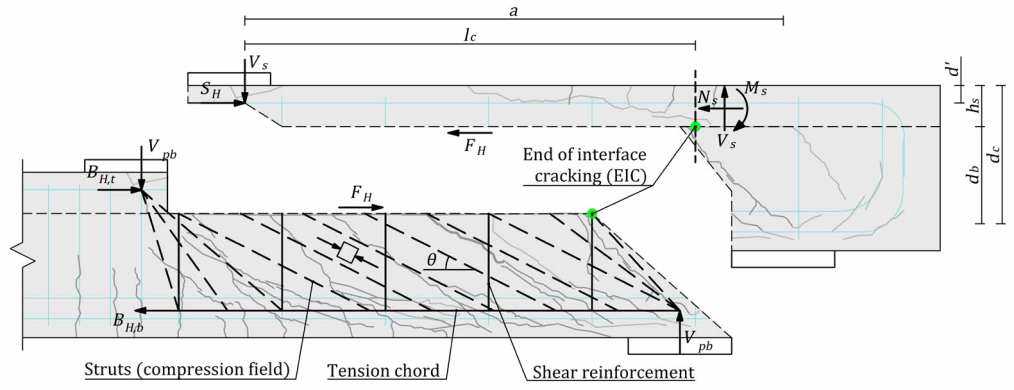

Figure 12. Diagram of the proposed model.

the sum of the web width (b_w) and once the flange depth (h_s) (see [25]). On the other hand, most of the specimens with extended interface cracking, which were composite specimens in this test programme, showed slab bending failure, and flanges did not increase shear strength.

By considering the observations related to the crack patterns, the shear strength mechanisms, and the effect of the varied parameters on shear strength, a mechanical model for explaining the shear resistant behaviour of the specimens with web reinforcement was proposed, which is described in Section 4.

4. PROPOSED MECHANICAL MODEL FOR EXPLAINING THE TEST RESULTS

A mechanical model was proposed for composite rectangular beams in [24], and extended to T-shaped beams in [25], based on the experimental observations, for explaining the shear behaviour of the specimens with web reinforcement of this experimental programme. In the model presented in [24,25], three variants of a strut-and-tie model were distinguished in the specimens tested. Each specimen was assigned one of these variants depending on their cracking patterns and other results from the instrumentation. The expressions for obtaining the shear strength of each variant were formulated for the geometry and reinforcement layout of the tested specimens.

In this paper, the three variants of the model presented in [24,25] are condensed into one unique formulation that is also generalised to geometries and reinforcement layout other than those tested by the authors, which is described below.

The model is based on the cracking of the weak plane, which was observed at the interface of composite specimens and at the cross-section width change in monolithic T-shaped specimens. So far, the model is applied to the specimens with one weak plane in the experimental programme.

The crack at the weak plane divides the shear transmission from the point load to the supports into two load paths: one through the beam web and one through the slab of the composite specimens or the flanges in T-beams (see Figure 12). The shear transmitted through the beam web is represented by a truss model where, according to the experimental results, the stirrups are considered yielded. The slab or the flanges are considered to transmit shear as a cantilever member without shear reinforcement. Both structures are connected at the interface crack, where horizontal forces are transferred due to the dowel action of the stirrups and the aggregate interlock [24,25].

The upper shear transmission path originated by the crack at the interface, whose length is l_c in Figure 12, is subjected to bending, axial and shear forces. While the shear at the slab or the flanges is considered to remain constant, the axial force decreases and the bending moment increases towards the support. Consequently, the weakest section is located at the end of the interface crack (EIC in Figure 12) and is likely to fail by bending or shear. This distribution of forces made it possible for flexural cracks to develop at the top of the slab, as observed in Figure 12. The observed behaviour of the slab was verified with the strain gauges located on top of the slab [25].

The shear strength of the specimen is obtained as the sum of the shear resisted by the beam web (V_{pb} in Figure 12) and the shear resisted by the slab or the flanges (V_s in Figure 12). The maximum shear force resisted by the beam web is governed by the yielding of the stirrups, so V_{pb} is calculated from

$$V_{pb} = \frac{T_w \, d_b \, cot\theta}{s} \quad (1)$$

where $T_w = A_{sw} \cdot f_{yw}$ is the tension force of the web reinforcement at its yield strength f_{yw}, A_{sw} is the cross-section area of the two legs of a stirrup, db is the effective depth of the precast beam (see Figure 12), θ is the inclination of the compression field in the web and s is the stirrup spacing. The horizontal force at the interface crack (F_H in Figure 12) can be obtained from the beam truss as

$$F_H = V_{pb} \frac{l_c}{d_b} \quad (2)$$

Based on the observations, the maximum shear capacity of the truss mechanism is reached prior to the specimen failure and the shear transferred by the truss mechanism may be assumed to remain constant for increasing loads. Thus, the failure of the specimen is governed by the slab failure. According to the observations, three slab failure modes can be identified (see Section 3.2.2): BF, SF and IF. Therefore, the shear strength resisted by the slab V_s is the minimum of the three values corre-

sponding to these three failure modes and the predicted shear strength V_{pred} of the specimen may be expressed as

$$V_{pred} = V_{pb} + V_s = V_{pb} + \min\{V_{s,BF}, V_{s,SF}, V_{s,IF}\} \quad (3)$$

BF is considered to occur when the slab longitudinal reinforcing steel reaches its yield strength in tension [24] at the EIC section (see Figure 12). Thus, $V_{s,BF}$ is obtained as

$$V_{s,BF} = \frac{F_H (h_s - d')\ d_b + T_l (h_s - d')(d_c - d')}{a\ d_b - (a - l_c)(d_c - d')} \quad (4)$$

where T_l is the tension force of slab longitudinal reinforcement at its yield strength. All other variables are defined in Figure 12.

The model considers the slab is subjected to a biaxial state of stresses, so SF occurs when the principal concrete stresses reach Kupfer's failure surface. Thus, $V_{s,SF}$ is obtained from the following formulae:

$$N_s = \frac{V_{s,SF}\ a - (h_s - d')\ F_H}{d_c - d'} \quad (5)$$

$$\sigma_x = -\frac{N_s}{b_{eff}\ h_s} \quad (6)$$

$$\begin{cases} \sigma_1 = \dfrac{\sigma_x}{2} + \sqrt{\left(\dfrac{\sigma_x}{2}\right)^2 + \tau^2} \le f_{ct,s} \\ \sigma_2 = \dfrac{\sigma_x}{2} - \sqrt{\left(\dfrac{\sigma_x}{2}\right)^2 + \tau^2} \le -f_{c,s} \\ \sigma_1 = |f_{ct,s}| + 0.8\,\dfrac{|f_{ct,s}|}{|f_{c,s}|}\,\sigma_2 \end{cases} \quad (7)$$

$$V_{s,SF} = 2/3\ \tau\ b_{eff}\ h_s \quad (8)$$

where N_s is the axial force in the slab at the EIC cross-section [24], b_{eff} is the effective shear width of the slab, which is taken as the web width in rectangular specimens and the sum of the web width and the flange depth in T-shaped specimens, which increases shear strength approximately in the same way as observed experimentally [25], σ_1 and σ_2 are the principal tensile and compression stresses from the normal force σ_x and the tangential force τ at the slab, $f_{c,s}$ and $f_{ct,s}$ are the concrete compressive and tensile strengths of the slab, respectively.

Finally, $V_{s,IF}$ is considered to occur when the remaining uncracked interface reaches its interface shear strength τ_R. Thus, $V_{s,IF}$ can be formulated as a function of the web width bw and the length of the uncracked interface lnc, measured from EIC to the end of the beam (see [25] for further explanation).

$$V_{s,IF} = \frac{\tau_R\ b_w\ l_{nc}(d_c - d') + F_H (h_s - d')}{a} \quad (9)$$

The shear strength of the specimens has been predicted with the proposed mechanical model, which requires using the length of the interface crack (l_c) observed in each specimen; the interface shear strength τ_R, taken as 1.9 MPa, which was a value calculated in [25] for these experimental results; and the experimental cotangent of the inclination of the compression field in the web ($\cot\theta$), taken as 2.13, which was calibrated in [24,25] for all the specimens of the experimental programme since it performs adequately in these specimens, which all have the same reinforcement layout. This $\cot\theta$ is slightly higher than the one obtained by taking an inclination of the compression field parallel to the diagonal cracks to account for the effect of aggregate interlock through the cracks.

The proposed mechanical model can accurately predict the failure mode of the tested specimens and their shear strengths. The results are shown in Figure 13. The model gives a mean value of the ratio V_{exp}/V_{pred} of 1.06 and a coefficient of variation (CV) of 7% for the 25 specimens of the experimental programme that showed an interface crack. Thus, the model proves useful for explaining the shear strength mechanisms developed by the specimens with web reinforcement of the experimental programme that showed horizontal cracking at the weak plane.

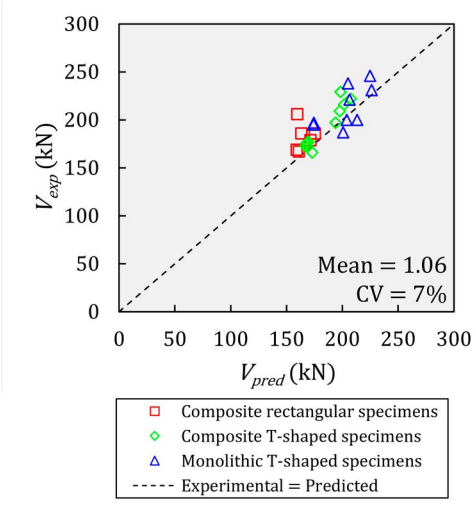

Figure 13. Experimental vs. Predicted shear strength of the 25 specimens from [24] and [25] that showed an interface crack, calculated with the proposed mechanical model for explaining the test results.

5. SHEAR STRENGTH PREDICTIVE FORMULATION FOR COMPOSITE BEAMS AND MONOLITHIC T-BEAMS WITH WEB REINFORCEMENT

The mechanical model described in Section 4 was proposed to assist in the analysis of the experimental results. However, it is not useful as a predictive formulation because it is based on certain experimental data taken from the tests themselves: the length of the interface crack (l_c) and the inclination of the compression field in the web θ.

The following formulation is a first attempt to simplify the model proposed in Section 4 and turn it into a predictive formulation. This topic is still being studied by the authors in order to provide a general user-friendly formulation for concrete composite beams.

5.1. Formulation

5.1.1. Calculation of V_{pb}

V_{pb} is obtained as in Eq. (1) by using the inclination angle of the compression field struts θ. In this formulation, $\cot\theta$

(see Eq. 10) may be limited by crushing of the compression struts ($\cot\theta_{str}$), in which case the formulation of EC2 [19] may be used (Eq. (11)). Additionally, the experimental observations described above show that the existence of a weak plane (interface or cross-section width change) may modify the inclination of the compression field of the web ($\cot\theta_{int}$). Consequently, the $\cot\theta$ may be also limited by the interface shear strength τ_R (Eq. (12)).

$$\cot\theta = \min\{\cot\theta_{str}, \cot\theta_{int}\} \tag{10}$$

$$1.0 \le \cot\theta_{str} = \sqrt{\frac{\nu\ f_{c,b}}{\rho_w\ f_{yw}} - 1} \le 2.5 \tag{11}$$

$$\cot\theta_{int} = \frac{\alpha\ \tau_R\ b_w s}{T_w} \ge 1 \tag{12}$$

where $f_{c,b}$ is the beam concrete compressive strength, ν is a strength reduction factor for concrete cracked in shear that may be taken from EC2 [19] (ν = 0.6·(1-$f_{c,b}$ /250), with $f_{c,b}$ in MPa), ρ_w is the shear reinforcement ratio, τ_R is calculated from EC2 [19] interface shear formulation (Eq. (13)) and α is a parameter that multiplies τ_R, which was calibrated in [19] with a large database of shear-transfer experiments, to use a more realistic value of the interface shear strength, given the very conservative predictions of the interface shear strength provided by the EC2 formulation that have been described in the literature [16,32,33]. The value of α for different interface roughness is given in Table 6.

$$\tau_R = c\ f_{ct} + \rho_{ic}\ f_{yw}\ \mu \le 0.5\ \nu\ f_c \tag{13}$$

The parameters c and μ in Eq. (13) are those defined in EC2 [19], which depend on the interface roughness, and are given in Table 6. f_c and f_{ct} are the minimum compressive and tensile strength of the two concretes of the composite beam. ρ_{ic} is the ratio of reinforcement crossing the interface.

TABLE 6.
Values of the factors c and μ defined in EC2 [19] and multiplier α for different interface roughness.

Interface roughness	c	μ	α
"Smooth" or "as cast"	0.2	0.6	1.9
"Rough" and "very rough"	0.4	0.7	1.3
Concrete placed monolithically	1.0	0.9	1.1

5.1.2. Calculation of V_s

Only two failure modes are considered in the simplified formulation due to the introduction of the interface shear strength: BF and SF.

The value of $V_{s,BF}$ in Eq. (4) is obtained by approximating the length of the interface crack (l_c) as the difference between the shear span a and the stirrup spacing s (Eq. (14)). In the same way, the horizontal force along the interface crack F_H is obtained from Eq. (15).

$$V_{s,BF} = \frac{F_H(h_s - d')\ d_b + T_l(h_s - d')(d_c - d')}{a\ \ d_b - s(d_c - d')} \tag{14}$$

$$F_H = V_{pb}\ \frac{a - s}{d_b} \tag{15}$$

When there is no longitudinal reinforcement in the slab, $V_{s,BF}$ may be derived from the concrete cracking moment at the slab end section [34] (Eq. (16)).

$$V_{s,BF} = \frac{F_H(h_s - d')\left(d_c - \frac{h_s}{3}\right) + \frac{f_{ct,s}}{6} b_{eff}\ h_s^2 (d_c - d')}{a\left(d_c - \frac{h_s}{3}\right) - s\ (d_c - d')} \tag{16}$$

where b_{eff} is the effective flange width defined in Section 5.3.2.1 of EC2 [19].

In specimens with slab longitudinal reinforcement, the maximum value of $V_{s,BF}$ from Eq. (14) and Eq. (16) should be considered.

On the other hand, the value of $V_{s,SF}$ is obtained from Eqs (5-8), where F_H is obtained from Eq. (15) and b_{eff} is considered as explained in Eq. (8), but not lower than that from Section 5.3.2.1 of EC2 [19].

5.1.3. Calculation of V_{pred}

V_{pred} is obtained in different ways depending on the shape of the cross-section and the presence of an interface between concretes.

If $\cot\theta_{int} \le \cot\theta_{str}$, an extensive cracking of the interface or the cross-sectional width change is likely to happen. Consequently, $V_{pred} = V_{pb} + \min\{V_{s,BF}, V_{s,SF}\}$.

On the contrary, if $\cot\theta_{int} > \cot\theta_{str}$, the specimen will behave as a monolithic specimen. In this last case, if the specimen has a rectangular cross-section, no cracks at the interface between concretes are expected. Therefore, the proposed formulation is not applicable since the model is based on the formation of a crack along the weak plane. Hence, its shear strength is obtained from current codes shear formulations for specimens with web reinforcement, such as that of EC2 [19], by using $f_{c,b}$ in calculating $\cot\theta$, since that equation accounts for the beam web stresses. If the specimen has a T-shaped cross-section, only the slab shear failure is considered, since a small extension of the interface crack will be expected, like in monolithic T-beams. Therefore, $V_{pred} = V_{pb} + V_{s,SF}$.

5.2. Experimental verification and comparison with existing code shear formulations

The proposed formulation is applied to 28 specimens with web reinforcement of the experimental programme: the 9 composite rectangular specimens with B2 cross-section and $\rho_{ic} = \rho_w$ = 0.22%; the 10 composite T-shaped specimens with C2 and D2 cross-section and web reinforcement; the 9 monolithic T-beams with C1 and D1 cross-section and web reinforcement. Additionally, 24 shear tests from the literature are taken to study the accuracy of the proposed model in predicting the shear strength of concrete composite beams: 9 composite specimens with rectangular cross-section from Halicka [14] and 15 composite specimens with T-shaped cross-section from Jabłoński & Halicka [15]. They have similar characteristics to B2 and D2 cross-sections in this paper, respectively, but different dimensions.

The results obtained are shown in Table 7. The composite rectangular specimens (CR), composite T-shaped specimens (CT) and monolithic T-beams (MT) of each author are divided into groups with the same characteristics of ρ_w, ρ_{ic} and interface roughness for comparison. The mean value of V_{exp}/V_{pred} and the CV are given for each group.

TABLE 7.
Mean and *CV* of V_{exp}/V_{pred} ratio for each group of assessed specimens with the proposed formulation.

ID Group	Reference	Nomenclature in their publication	ρ_w (%)	ρ_{ic} (%)	Interface roughness	No. of specimens	Mean	CV (%)
CR1	Rueda-García *et al.* [22]	NWP1B2i	0.22	0.22	Rough	1	1.15	-
CR2	Rueda-García *et al.* [24]	NWPzB2	0.22	0.22	Smooth	8	1.18	7.71
CR3	Halicka [14]	CB/A+S	0.42	0.21	Rough	3	1.22	4.56
CR4	Halicka [14]	CB/A	0.42	0	Rough	3	1.26	4.70
CR5	Halicka [14]	CB/S	0.42	0.21	Smooth	3	1.04	4.01
CT1	Rueda-García *et al.* [25]	NWPzC2; NWPzD2	0.22	0.22	Smooth	10	1.17	9.43
CT2	Jabłoński & Halicka [15]	BZ/P+S; BZ/S1	0.42	0.21	Rough	6	1.54	4.57
CT3	Jabłoński & Halicka [15]	BZ/P	0.42	0	Rough	3	1.03	5.66
CT4	Jabłoński & Halicka [15]	BZ/S2/A	0.42	0.21	Smooth	3	1.41	5.45
CT5	Jabłoński & Halicka [15]	BZ/S2/B	0.42	0.42	Smooth	3	1.30	1.38
MT1	Rueda-García *et al.* [25]	NWPzC1; NWPzD1	0.22	0.22	Monolithic	9	0.99	7.62

Table 7 shows that the mean values of V_{exp}/V_{pred} are in general close to the unit for each group. Some groups of specimens, such as CT2, CT4 or CT5 show higher mean values. However, the coefficients of variation are very low for each group of beams. This shows that the proposed formulation adequately captures the resistance mechanism.

Furthermore, the shear strengths predicted by the proposed formulation are compared with those of current codes formulations for beams with shear reinforcement. In this comparison, EC2 [19], the Level III Approximation of MC-10 [20] and the formula (b) of ACI 318-19 [21] (Section 22.5.5.1) are considered. Current codes do not account for the composite action unless the interface shear strength meets the code requirements. Therefore, for this comparison, the interface shear strength of the specimens is first checked according to the code formulation. The predicted shear strength is that of only the precast beam if the interface shear strength is not verified. On the contrary, the minimum shear strength given by the interface strength and that given by the entire composite beam depth is taken, as in [34].

Figure 14 compares the shear strength predicted by the proposed formulation for the 52 considered specimens with those of the three current codes. As observed, the proposed model gives the best approximation to the experimental values, with the lowest CV. EC2 [19] provides que best results of the three considered codes, even though the code provides the same shear strength for all the specimens of the same group of beams since the concrete compressive strength is not considered. On the other hand, MC-10 [20] and ACI 318-19 [21] give very similar results but far from the test values.

The proposed formulation has proven its accuracy in the prediction of the shear strength of the specimens of this experimental work, from which it was developed, and other specimens with similar characteristics from the literature. However, further studies should be conducted in future to check its suitability in a larger database of specimens of different characteristics and to fix its application boundaries and its limitations. An adaptation of the proposed model would be needed to use it in the tested T-beams with top cast-in-place slab (series E2 and F2 in Figure 2), given the presence of two weak planes that modify the shear transfer mechanisms, which is one of the future research lines of this work.

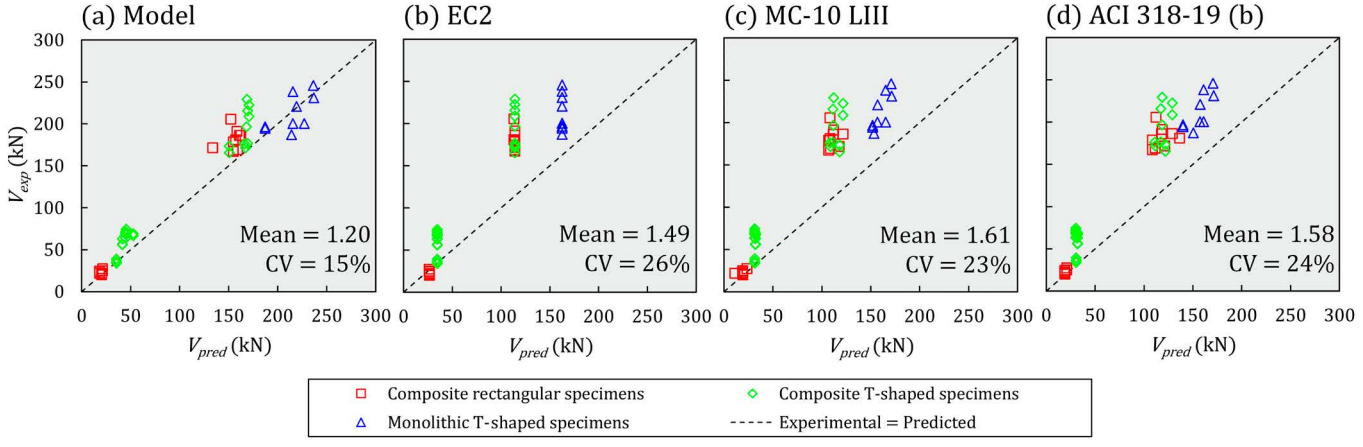

Figure 14. Experimental vs. Predicted shear strength of the 52 analysed specimens with different shear formulations: (a) Proposed formulation; (b) EC2 [19]; (c) MC-10 Level III [20]; (d) ACI 318-19 (b) [21].

6. CONCLUSIONS

This paper presents the experimental work carried out to study the shear strength of concrete composite beams in which different parameters were varied. The shear strength mechanisms of the 69 test specimens and the effect of various test parameters on shear strength were analysed, from which multiple conclusions were drawn. Furthermore, based on the experimental observations, a shear strength model was proposed for explaining the test results, which was also transformed into a predictive shear strength formulation that gave accurate results. The most relevant aspects to be highlighted from this research are:

1. When the composite specimens are designed to avoid the horizontal shear failure, the interface usually modifies the crack patterns, by forcing them to develop along the interface before penetrating the slab. These specimens show two shear transmission paths: one through the precast beam web; and another through the cast-in-place slab.
2. In elements without shear reinforcement, the shear strength (first local maximum shear value) is mainly related to the shear transferred through the web. Consequently, the concrete compressive strength of the slab and the existence of flanges in T-shaped beams do not have a major impact on the shear strength.
3. In members with shear reinforcement, the ductile behaviour of the web allows the contribution of the two shear transfer mechanisms to be added to calculate the shear strength of the composite beam. Depending on the interface shear strength, the failure of the slab will be by shear or by flexure. In case of slab shear failure, the shear strength of the specimen will depend on the concrete strength of the slab and its width. On the contrary, the slab shear strength will mainly depend on the strength of the longitudinal reinforcement of the slab. Based on the variable angle truss mechanism to transfer the shear force through the web, the concrete strength of the beam will influence the shear strength of the specimen by limiting the inclination of the compression field.
4. In monolithic T-beams, the horizontal plane where the width changes has a similar influence on the crack pattern as that of a concrete-to-concrete interface in composite beams, since diagonal cracks propagate along it. Therefore, two shear paths are also observed in the tests carried out in this experimental programme and the proposed model has been proved useful to predict their shear strength.

This research work shows a large number of experimental results and a detailed analysis of the shear strength mechanisms of concrete composite beams. However, further research should be conducted on specimens of other dimensions and characteristics to get a more general and user-friendly shear strength formulation for composite elements.

Acknowledgements

Ministerio de Ciencia e Innovación (MCIN) and *Agencia Estatal de Investigación* (AEI) supported the present research work through grants BIA2015-64672-C4-4-R and RTI2018-099091-B-C21-AR, both funded by MCIN/AEI/ 10.13039/501100011033 and by "ERDF A way of making Europe". Author Lisbel Rueda-García was supported by grant BES-2016-078010 funded by MCIN/AEI/ 10.13039/501100011033 and by "ESF Investing in your future". The project was also carried out with the support of the Regional Government of Valencia through Project AICO/2018/250. This research work was undertaken at the Concrete Science and Technology University Institute (ICITECH) of the Universitat Politècnica de València (UPV; Spain) with concrete supplied by Caplansa.

Competing Interests

All authors certify that they have no affiliations with or involvement in any organization or entity with any financial interest or non-financial interest in the subject matter or materials discussed in this manuscript.

References

[1] A. Halicka, Ł. Jabłoński, Shear failure mechanism of composite concrete T-shaped beams, Proc. Inst. Civ. Eng. - Struct. Build. 169 (2016) 67–75. https://doi.org/10.1680/stbu.14.00127.

[2] C.R. Ribas González, M. Fernández Ruiz, Influence of flanges on the shear-carrying capacity of reinforced concrete beams without web reinforcement, Struct. Concr. (2017). https://doi.org/10.1002/suco.201600172.

[3] J.C. Saemann, G.W. Washa, Horizontal Shear Connections between Precast Beams and Cast-in-Place Slabs, ACI J. Proc. 61 (1964) 1383–1409.

[4] R.E. Loov, A.K. Patnaik, Horizontal Shear Strength of Composite Concrete Beams With a Rough Interface, PCI J. 39 (1994) 48–69. https://doi.org/10.15554/pcij.01011994.48.69.

[5] K.H. Tan, L.W. Guan, X. Lu, T.Y. Lim, Horizontal shear strength of indirectly loaded composite concrete beams, ACI Struct. J. 96 (1999) 533–538. https://doi.org/10.14359/689.

[6] L.F. Kahn, A. Slapkus, Interface Shear in High Strength Composite T-Beams, PCI J. 49 (2004) 102–110. https://doi.org/10.15554/pcij.07012004.102.110.

[7] J. Kovach, C. Naito, Horizontal Shear Capacity of Composite Concrete Beams without Interface Ties, ATLSS Report No. 05-09, 2008.

[8] Z. Fang, H. Jiang, A. Liu, J. Feng, Y. Chen, Horizontal Shear Behaviors of Normal Weight and Lightweight Concrete Composite T-Beams, Int. J. Concr. Struct. Mater. 12 (2018). https://doi.org/10.1186/s40069-018-0274-3.

[9] C.-G. Kim, H.-G. Park, G.-H. Hong, S.-M. Kang, Shear strength of composite beams with dual concrete strengths, ACI Struct. J. 113 (2016) 263–274. https://doi.org/10.14359/51688061.

[10] M.A. Shahawy, B. deV Batchelor, Shear Behavior of Full-Scale Prestressed Concrete Girders: Comparison Between AASHTO Specifications and LRFD Code, PCI J. 41 (1996) 48–62. https://doi.org/10.15554/pcij.05011996.48.62.

[11] H.R. Hamilton III, G. Llanos, B.E. Ross, Shear performance of existing prestressed concrete bridge girders, 2009.

[12] B. Runzell, C. Shield, C. French, Shear Capacity of Prestressed Concrete Beams, 2007.

[13] D.L. Hartmann, J.E. Breen, M.E. Kreger, Shear capacity of high strength prestressed concrete girders, Austin, 1988.

[14] A. Halicka, Influence new-to-old concrete interface qualities on the behaviour of support zones of composite concrete beams, Constr. Build. Mater. (2011) 4072–4078. https://doi.org/10.1016/j.conbuildmat.2011.04.045.

[15] Ł. Jabłoński, A. Halicka, Influence of the interface reinforcement on static performance of concrete composite T-shaped beams, Bud. i Archit. 19 (2020) 063–076. https://doi.org/10.35784/bud-arch.2170.

[16] C.-G. Kim, H.-G. Park, G.-H. Hong, S.-M. Kang, H. Lee, Shear Strength

of Concrete Composite Beams with Shear Reinforcements, ACI Struct. J. 114 (2017) 827–837. https://doi.org/10.14359/51689441.

[17] C.-G. Kim, H.-G. Park, G.-H. Hong, H. Lee, J.-I. Suh, Shear strength of RC-composite beams with prestressed concrete and non-prestressed concrete, ACI Struct. J. 115 (2018). https://doi.org/10.14359/51702224.

[18] C.-G. Kim, H.-G. Park, G.-H. Hong, S.-M. Kang, Shear strength of composite beams with steel fiber-reinforced concrete, ACI Struct. J. 116 (2019). https://doi.org/10.14359/51716812.

[19] CEN, EN 1992-1-1:2013. Eurocode 2: Design of concrete structures - Part 1-1: General rules and rules for buildings (revised version 2020), 2020.

[20] Fédération International du Béton (fib), Model Code 2010, Ernst & Sohn, 2012.

[21] ACI Committee 318, 318-19(22): Building Code Requirements for Structural Concrete and Commentary (Reapproved 2022), American Concrete Institute, 2022.

[22] L. Rueda-García, J.L. Bonet Senach, P.F. Miguel Sosa, Influence of interface roughness and shear reinforcement ratio in vertical shear strength of composite concrete beams, Hormigón y Acero. 73 (2022). https://doi.org/10.33586/hya.2022.SANTANDER.

[23] L. Rueda-García, J.L. Bonet Senach, P.F. Miguel Sosa, M.Á. Fernández Prada, Experimental analysis of the shear strength of composite concrete beams without web reinforcement, Eng. Struct. 229 (2021) 111664. https://doi.org/10.1016/j.engstruct.2020.111664.

[24] L. Rueda-García, J.L. Bonet Senach, P.F. Miguel Sosa, M.Á. Fernández Prada, Analysis of the shear strength mechanism of slender precast concrete beams with cast-in-place slab and web reinforcement, Eng. Struct. 246 (2021) 113043. https://doi.org/10.1016/j.engstruct.2021.113043.

[25] L. Rueda-García, J.L. Bonet Senach, P.F. Miguel Sosa, M.Á. Fernández Prada, Experimental study on the shear strength of reinforced concrete composite T-shaped beams with web reinforcement, Eng. Struct. 255 (2022) 113921. https://doi.org/10.1016/j.engstruct.2022.113921.

[26] M.W. Kani, Mark W. Huggins, Rudi R. Wittkopp, Kani on shear in reinforced concrete, University of Toronto, Dept. of Civil Engineering, Toronto, 1979.

[27] M. Fernández Ruiz, A. Muttoni, J. Sagaseta, Shear strength of concrete members without transverse reinforcement: A mechanical approach to consistently account for size and strain effects, Eng. Struct. 99 (2015) 360–372. https://doi.org/10.1016/j.engstruct.2015.05.007.

[28] UNE-EN 12390-3:2020, Testing hardened concrete - Part 3: Compressive strength of test specimens, 2020.

[29] UNE-EN 12390-6:2010, Testing hardened concrete - Part 6: Tensile splitting strength of test specimens, 2010.

[30] UNE-EN 12390-13:2014, Testing hardened concrete - Part 13: Determination of secant modulus of elasticity in compression, 2014.

[31] UNE-EN ISO 6892-1:2017, Metallic materials - Tensile testing - Part 1: Method of test at room temperature, 2017.

[32] M. Soltani, B.E. Ross, Database evaluation of interface shear transfer in reinforced concrete members, ACI Mater. J. 114 (2017) 383–394. https://doi.org/10.14359/51689249.

[33] L. Rueda, J.L. Bonet, P.F. Miguel, Experimental study of concrete composite beams subjected to shear, in: Proc. Fib Symp. 2019 Concr. - Innov. Mater. Des. Struct., 2019.

[34] L. Rueda-García, Experimental Assessment of the Shear Resistant Behaviour of Precast Concrete Beams with Top Cast-in-Place Concrete Slab, Universitat Politècnica de València, 2022. https://doi.org/10.4995/Thesis/10251/183594.